ORIGINAL ARTICLE

In vivo positron emission tomography imaging with [^{11}C]ABP688: binding variability and specificity for the metabotropic glutamate receptor subtype 5 in baboons

**Christine DeLorenzo · Matthew S. Milak ·
Kathleen G. Brennan · J. S. Dileep Kumar ·
J. John Mann · Ramin V. Parsey**

Abstract

Purpose Metabotropic glutamate receptor subtype 5 (mGluR5) dysfunction has been implicated in several disorders. [^{11}C]ABP688, a positron emission tomography (PET) ligand targeting mGluR5, could be a valuable tool in the development of novel therapeutics for these disorders by establishing in vivo drug occupancy. Due to safety concerns in humans, these studies may be performed in nonhuman primates. Therefore, in vivo characterization of [^{11}C]ABP688 in nonhuman primates is essential.

Methods Test–retest studies were performed in baboons (*Papio anubis*) to compare modeling approaches and determine the optimal reference region. The mGluR5-specific antagonist 3-((2-methyl-1,3-thiazol-4-yl)ethynyl) pyridine (MTEP) was then used in test–block studies, in which ligand binding was measured before and after MTEP administration. Test/block data were analyzed both by calculating changes in binding and using a graphical approach, which allowed estimation of both MTEP occupancy and nonspecific binding.

Results Test–retest results, which have not been previously reported for [^{11}C]ABP688, indicated that [^{11}C]ABP688 variability is low using an unconstrained two-tissue compartment model. The most appropriate, though not ideal, reference region was found to be the gray matter of the cerebellum. Using these optimal modeling techniques on the test/block data, about 90% occupancy was estimated by the graphical approach.

Conclusion These studies are the first to demonstrate the specificity of [^{11}C]ABP688 for mGluR5 with in vivo PET in nonhuman primates. The results indicate that, in baboons, occupancy of mGluR5 is detectable by in vivo PET, a useful finding for proceeding to human studies, or performing further baboon studies, quantifying the in vivo occupancy of novel therapeutics targeting mGluR5.

Keywords [^{11}C]ABP688 · Glutamate · Metabotropic glutamate receptor subtype 5 · MTEP · Positron emission tomography · Occupancy

C. DeLorenzo (✉) · M. S. Milak · K. G. Brennan ·
J. S. D. Kumar · J. J. Mann · R. V. Parsey
Division of Molecular Imaging and Neuropathology,
Department of Psychiatry, Columbia University College
of Physicians and Surgeons,
NYSPI Mail Unit 42, 1051 Riverside Drive,
New York, NY, USA
e-mail: cd2415@columbia.edu

M. S. Milak · J. S. D. Kumar · J. J. Mann · R. V. Parsey
New York State Psychiatric Institute,
New York, NY, USA

J. S. D. Kumar · J. J. Mann
Department of Radiology, Columbia University
College of Physicians and Surgeons,
New York, NY, USA

Introduction

Glutamate is the primary excitatory neurotransmitter in the brain [1]. Metabotropic glutamate (mGlu) receptors, a family of eight G-protein-coupled receptors, modulate glutamatergic transmission via second messenger signaling pathways [2, 3]. These receptors are divided into three groups based on their structure and function [2, 3]. Group I mGlu receptors (mGlu receptor subtypes 1 and 5, mGluR1

and mGluR5) regulate neuronal excitability indirectly by modulating glutamatergic transmission through *N*-methyl-*d*-aspartic (NMDA) receptors [4].

Dysfunction in mGluR5 (also referred to as the mGlu5 receptor) has been implicated in disorders such as schizophrenia [5–7], psychostimulant addiction [8, 9], Parkinson's disease [10–12], attention-deficit and hyperactivity disorder [13], and degenerative and dysplastic diseases of the central nervous system [14]. Altered mGluR5 is also suspected in the most common inherited form of mental retardation and autism, fragile X syndrome [15]. As such, mGluR5 may represent a viable therapeutic target for these disorders. For example, positive allosteric modulators of mGluR5 are currently being investigated as potential antipsychotic treatments for schizophrenia [16, 17], while mGluR5 antagonists are being examined in clinical trials for patients with fragile X syndrome [18].

Attention has also been focused on mGluR5 due to its role in anxiety and depression [2]. The effectiveness of mGluR5 antagonists as antidepressants has been assessed in several rodent studies. In both the tail suspension test [19] and forced swim test [20] paradigms, two different mGluR5 antagonists, MPEP (2-methyl-6-(phenylethynyl)-pyridine) and MTEP (3-((2-methyl-1,3-thiazol-4-yl)ethynyl)pyridine), exerted antidepressant-like effects in mice [21–23]. In a modified forced swim test, these effects (tested only with MTEP) were also noted in rats [21]. In addition, in a third paradigm in which olfactory bulbectomies were performed to induce depression-like behavior in rats, chronic administration of either MPEP [24, 25] or MTEP [22] reduced bulbectomy-induced behaviors.

Further evidence of the role of mGluR5 in the transduction of antidepressants came from mGluR5 knockout mice. Three key findings by Li et al. [23] were: (1) mGluR5 knockout mice have decreased immobility, i.e. an antidepressant-like effect, in the forced swim test; (2) MPEP is ineffective in mGluR5 knockout mice; but (3) the tricyclic antidepressant, imipramine, can still produce an antidepressant effect. The last finding suggests that mGluR5 blockade can enhance the efficacy of other antidepressants, either directly, by acting synergistically with these drugs, or through an independent pathway of antidepressant-like action.

Antagonists of mGluR5 have also exhibited the most robust and extensive anxiolytic activity, with the exception of benzodiazepines, in preclinical trials [26]. A large body of consistent evidence has revealed the effectiveness of both MTEP and MPEP, as well as several other mGluR5 antagonists, in inducing anxiolytic-like effects in rodents [2]. In addition, fenobam, a selective mGluR5 antagonist [27], produced an anxiolytic effect in patients with moderate to severe anxiety in a phase II double-blind study performed in the 1980s [28]. (Despite its clinical efficacy and absence of side effects commonly associated with benzodiazepines,

initial clinical trials of fenobam were discontinued due to psychostimulant adverse effects [2, 27].)

As underscored by the above evidence, mGluR5 is a potential therapeutic target for multiple disorders, and, as such, it is necessary to establish accurate methods for quantifying mGluR5 occupancy in vivo. This can be accomplished using PET and the ligand [11C]ABP688 (3-(6-methylpyridin-2-ylethynyl)cyclohex-2-enone-*O*-11C-methyl-oxime), which targets mGluR5 [29]. In vitro binding assays and biodistribution studies have shown that: at concentrations up to 10 μM, ABP688 does not bind to receptors or transporters other than mGluR5 [26] and that [11C]ABP688 uptake is significantly lower in mGluR5 knockout mice [29].

Although these in vitro studies indicate the probable in vivo specificity of [11C]ABP688 for mGluR5, this specificity must be quantitatively validated, due to differences in ligand kinetics, membrane integrity, temperature, pH, and the availability of guanosine triphosphate (GTP) between in vitro and in vivo conditions. In addition, it is important to note that both MPEP and MTEP are negative allosteric modulators and therefore require an orthosteric ligand to achieve modulation in vitro [35, 36], whereas, in vivo, MPEP or MTEP modulation can occur in the presence of endogenous glutamate. For these reasons, differences in sensitivity between in vitro and in vivo techniques may exist, and it is therefore important to establish: (1) that mGluR5 occupancy can be measured by in vivo techniques, and, if so, (2) the optimal methods to quantify that occupancy.

Initial studies of mGluR5 in vivo specificity have been performed in rodents. PET studies in the rat have shown that both the mGluR5 antagonist, MPEP, and methoxy substituted derivative of MPEP, 2-methyl-6-((3-methoxy-phenyl)ethynyl)pyridine (M-MPEP) [30], can induce significant reductions in [11C]ABP688 binding [29, 31, 32], and that injecting stable ABP688 following the M-MPEP administration does not result in further binding reductions [32]. Further, PET studies performed in mGluR5 knockout mice have shown homogeneous accumulation throughout the brain, with similar binding in the forebrain and cerebellum [29]. These findings are consistent with the results of initial human studies indicating increased uptake of [11C]ABP688 in mGluR5-rich regions [33, 34].

In order to perform specificity studies in humans, however, it is necessary to establish that physiologically tolerable doses of a highly specific mGluR5 blocking agent can produce a measurable blockade. As such, both rodent and baboon studies are a necessary precursor for human analysis. Although [11C]ABP688 blocking studies have been performed in rodents, this type of blocking study has never been performed in baboons, or using the highly specific mGluR5 antagonist, MTEP. In addition, a [11C] ABP688 test–retest study, the only method for assessing within-subject variability, has not been performed in any

species to date. Test–retest studies provide the best standard to assess modeling techniques, including choice of reference region. Therefore, in this work, a test–retest study was performed in baboons (*Papio anubis*) to confirm the optimal modeling technique for [^{11}C]ABP688, and to find an appropriate reference region. (Proper choice of reference region is essential for accurate quantification of occupancy using reference tissue approaches.) Using these optimal modeling techniques, the ability of the MTEP to displace [^{11}C]ABP688 from binding to mGluR5 was studied. MTEP occupancy was assessed in two ways, using the standard percent difference in binding, and with a graphical approach that does not require a reference region [37]. By comparing these two approaches, the optimal method to assess in vivo occupancy using [^{11}C]ABP688, and the effect of a non-ideal reference region on [^{11}C]ABP688 occupancy calculations, was determined. The results of these studies provide essential information for using this ligand in drug occupancy studies in the baboon, and are a necessary precursor for establishing [^{11}C]ABP688 in vivo specificity and occupancy in humans.

Materials and methods

[^{11}C]ABP688 synthesis

Radiosynthesis of [^{11}C]ABP688 was achieved using a procedure previously described [29], with slight modification. [^{11}C]MeOTf was trapped into an acetone (400 ml) solution containing 0.5 mg of desmethyl-ABP688 and 10 μl NaOH (5 N) at room temperature for 5 min. The crude product was loaded into a semipreparative HPLC column (C18; Phenomenex, Torrence, CA), eluted with 50:50 (acetonitrile/0.1 M AMF, 10 ml/min), and the product fraction (major diastereomer) was collected between 9 and 10 min, based on a γ-detector. The collected fraction was then diluted with 100 ml deionized water, passed through a C-18 SepPak (Waters, Milford, MA), and washed with water (2×20 ml). Following the water rinse, the product was eluted from the SepPak column with 1 ml ethanol. The ethanol solution was diluted with 9 ml normal saline and filtered through a 0.22 μm filter. A small portion of the product was analyzed by analytical HPLC for chemical and radiochemical purities, specific activity, and other quality control indices. The total time required for the synthesis of [^{11}C]ABP688 was 30 min from the end of bombardment. The average yield was 25±5% at the end of synthesis, and the mean specific activity of the product was 4.0±1.5 Ci/μmol.

Animal preparation and imaging

Two healthy male baboons (*P. anubis*) were studied according to protocols approved by the Columbia-Presbyterian Medical Center Animal Care and Use Committee. Animals were prepared and monitored as described previously [38].

Two types of PET studies were performed: test–retest (*n*=3) and test–block (*n* = 3). In the test–retest studies, performed twice on baboon 1 and once on baboon 2, the anesthetized baboon was scanned twice under the same conditions in a single day, separated by a break of approximately 1 h. In the test–block studies, also performed twice on baboon 1 and once on baboon 2, the anesthetized baboon was again scanned twice in a single day, separated by a break of approximately 1 h. However, before the second (block) scan, MTEP was injected as an intravenous bolus over 12 min. A minimal effective MTEP dose (1 mg/kg), based on previous studies was chosen. (Rodent studies have shown that 50% of mGluR5 receptors remain occupied 1 h after administration of 1 mg/kg MTEP [39, 40], and preclinical studies have indicated that 1 mg/kg MTEP can produce an anxiolytic response [41] and, in some paradigms, an antidepressant effect [22].) The baboon was then carefully monitored for hemodynamic stability (about 8–12 min after MTEP administration) before ligand injection and PET imaging.

PET imaging was performed with an ECAT EXACT HR+ (Siemens/CTI, Knoxville, TN) (63 slices covering an axial field of view of 15.5 cm, axial sampling of 2.425 mm, in 3-D mode). A 10-min transmission scan was acquired before injection. At the end of the transmission scan, [^{11}C]ABP688 was administered intravenously as a bolus over 45 s. Following injection of [^{11}C]ABP688, emission data were collected for 120 min as 23 successive frames of increasing duration (2×30 s, 3× 1 min, 5×2 min, 4×4 min, 9×10 min). Images were reconstructed using attenuation correction from the transmission data using a previously outlined procedure [42].

An MR image of each baboon's brain had been previously obtained for anatomical delineation. PET-to-MRI transformations were computed between the baboon's MR image and the mean image of frames four through nine of the PET scan, using FLIRT (FMRIB linear image registration tool), version 5.0 (FMRIB Image Analysis Group, Oxford, UK), with a mutual information cost function, six degrees of freedom, and trilinear interpolation. These early PET frames were chosen for coregistration because they portray the cerebral perfusion pattern, which is spatially similar to the MR image. Regions of interest (ROIs) were manually drawn on the corresponding MR image. Cerebellar gray matter was drawn on several MR slices as a cylindrical ROI within the cerebellum, at least one full-with at half-maximum distance from the white matter and the vermis. The volume of the cerebellar gray matter (105 and 100 mm^3 for baboons 1 and 2, respectively) was considerably smaller than that of the full cerebellum (11,010 and 5,829 mm^3, respectively). All ROIs were transferred to the PET frames using the coregistration transformation, and time–activity curves (TACs) were constructed using the measured ROI activity within each frame.

Input function measurement

Arterial samples were collected automatically every 10 to 20 s for the first 4 min, then manually for a total of 34 samples. The radioactivity in 200-μl aliquots of centrifuged plasma samples was measured in a 1480 Wizard 3 M automatic γ counter (Waallac, Turku, Finland). The free fraction was measured using an ultrafiltration technique as previously described [43]. However, due to the high protein binding of ABP688 [26], the accuracy of this technique was compromised by nonspecific binding to the apparatus [44]. Measuring plasma free fraction using equilibrium dialysis [45] is one way to potentially circumvent this problem in the future. Blood samples drawn at 2, 4, 12, 30, 60, and 90 min were further processed by HPLC for metabolite analysis.

Unmetabolized parent fraction levels were fitted to a Hills function [46]. The input function was calculated as the product of the interpolated parent fraction and the total plasma counts. These combined data were then fitted as the combination of a straight line and the sum of three exponentials, describing the function before and after the peak, respectively.

Outcome measure calculation

The outcome measure closest to the receptor density is BP_F (B_{avail}/K_D), where B_{avail} is the density of available receptors and K_D is the equilibrium dissociation constant [47]. Since the calculation of BP_F requires accurate measurement of the free fraction (f_p) and [^{11}C]ABP688 free fraction measurements were unreliable, BP_F estimations were unreliable. Therefore, in this work, the measurement closest to receptor density, while maintaining reliability, was BP_P (B_{max}/K_D * f_p). BP_P can be calculated as $(V_T−V_{ND})/V_{ND}$, where V_T is the volume of distribution (ratio of the concentration of the ligand in the region to that in the plasma at equilibrium) and V_{ND} is the volume of distribution of the reference region, representing the nondisplaceable V_T. Although BP_P is the outcome measure of choice when the free fraction is not measured, the advantage of using V_T as an outcome measure is that it is not influenced by estimations of V_{ND}.

When using reference region approaches, estimation of V_T and BP_P is not possible. In these cases, the outcome measure $BP_{ND}=f_{ND}B_{avail}/K_D$, where f_{ND} is the fraction of free ligand in the reference region, was used as it does not require blood sampling.

Modeling comparison

The modeling procedures considered have been previously reported [43], and can be separated into two types – kinetic and graphical. As previously performed [43], one-tissue compartment and two-tissue compartment (2TC) models

were calculated, both iteratively and noniteratively. Using noniterative methods, the experimental data are matched to the most similar curve in a library of precalculated functions, rather than performing a nonlinear least squares iterative fit. These approaches are therefore faster and less computationally expensive. An iterative 2TC constrained algorithm was also tested, in which the ratio of kinetic constants, K_1/k_2, for each ROI is constrained to the ratio of K_1/k_2 in the reference region [48]. Graphical methods were the second type of approach used. Using Logan graphical analysis, outcome measures can be calculated from the slope of the linear part of an integral plot [49]. The linear portion of the graph for [^{11}C]ABP688 was considered to be the last eight points. To reduce the bias introduced by the Logan approach [50], likelihood estimation in graphical analysis was also used [51]. In addition to these methods, two methods that do not require blood sampling were applied – the simplified reference tissue model (SRTM) [52], and a bloodless version of the Logan method [53] to determine the effect of reference tissue assumptions on outcome measure, and therefore occupancy measures.

Five outcome metrics were used to assess the performance of each modeling approach. These metrics, which have been previously defined [43], are:

1. Percent difference (PD), measuring the absolute difference between test and retest values in the same subject, divided by their average.
2. Within subject mean sum of squares (WSMSS), which indicates the variance of an outcome measure based on repeated measurements in the same subject.
3. Variance, the square of the standard deviation of the value across subjects.
4. Intraclass correlation coefficient (ICC), which determines how much variability is due to differences between subjects as opposed to within the same subject. This measure varies between −1 and 1.
5. Identifiability (ID), measuring the stability of the estimate, based on bootstrap samples of the TACs of each subject [54]. Lower identifiability indicates more stable data.

Results

Baboon metabolism

Metabolism was rapid with the percentage of unmetabolized [^{11}C]ABP688 decreasing quickly in the first 10 min. However, since radiolabeled metabolites of [^{11}C]ABP688 are more hydrophilic than the parent compound, these metabolites are unlikely to cross the blood–brain barrier [33]. The average percent parent compound across all 12

studies at 2, 4, 12, 30, 60, and 90 min was: 89.39±4.57, 61.18±11.60, 23.32±8.79, 17.04±3.47, 15.91±2.55, and 15.65±2.58, respectively. The initial, retest, and block mean injected doses were comparable (5.40±0.86, 5.53±0.80, and 5.45±0.80 mCi, respectively).

Regional uptake

In order to create images of regional uptake with less noise, voxel maps of regional binding were combined and averaged. To accomplish this, all images from the test–retest study ($n=6$), as well as baseline scans from the test–block experiments ($n=3$) were first transformed to the space of their corresponding MR images using the calculated coregistration transform. The MR image of baboon 2 was then nonlinearly warped to the MR image of baboon 1 using the Automatic Registration Toolbox [55], and the resulting nonlinear transform was used to bring each V_T voxel map of baboon 2 into the same space as the V_T voxel maps of baboon 1 (top row of Fig. 1).

Regional uptake was greater in regions of the brain with known distributions of mGluR5 such as the insula, amygdala, caudate, temporal lobe, putamen, and hippocampus. Lower binding was observed in the thalamus, occipital lobe, and cerebellum.

Test–retest results: modeling methods comparison

The results of test–retest model comparison are presented in Table 1. Since the one-tissue compartment models (both iterative and noniterative) did not fit the data well, these models were excluded from Table 1 and further analysis. Among the 2TC models and graphical approaches, outcome metrics were not strongly sensitive to model choice. However, the unconstrained 2TC modeling method was identified as the optimal model since it attained the lowest percent difference, WSMSS, and variance (although the constrained 2TC model attained a slightly lower standard deviation of the variance), and highest ICC.

Although a similar metric comparison performed using BP_P did not yield a top performer (no one method performed best in multiple categories), the 2TC method also performed well in BP_P comparisons (PD 11.69±6.10%, WSMSS 0.05±0.02 (ml/cm³)², ICC 0.61±0.27, variance 0.13±0.04 ml/cm³, ID 0.59±0.27 ml/cm³). For this reason, the unconstrained 2TC modeling method was used for the test–block studies.

Test–block results

As indicated in the middle row of Fig. 1, MTEP extensively blocked the uptake of [¹¹C]ABP688. The difference between [¹¹C]ABP688 binding under baseline and block conditions was also apparent from individual TACs (Fig. 2).

Figure 3 shows the percentage block (gray bars) achieved in all regions examined. Both the entire cerebellum and the cerebellar gray matter (CGM) are shown. The region with the smallest percentage difference between baseline and block conditions was the CGM. However, even this region showed an average decrease in binding of about 7% between baseline and block conditions.

Fig. 1 Mean PET images under normal (*top row*) and block (*middle row*) conditions, and MR images (*bottom row*, baboon 1, for anatomical reference). Coronal, sagittal, and axial views of the baboon brain are shown (*left*, *middle*, *right*, respectively). For each PET image acquired under normal conditions (i.e. without administration of MTEP, $n=9$) or under block conditions ($n=3$), the volume of distribution (V_T) was calculated at every voxel using the Logan graphical approach [49]. The mean of each set of V_T voxel maps is shown (see text for explanation)
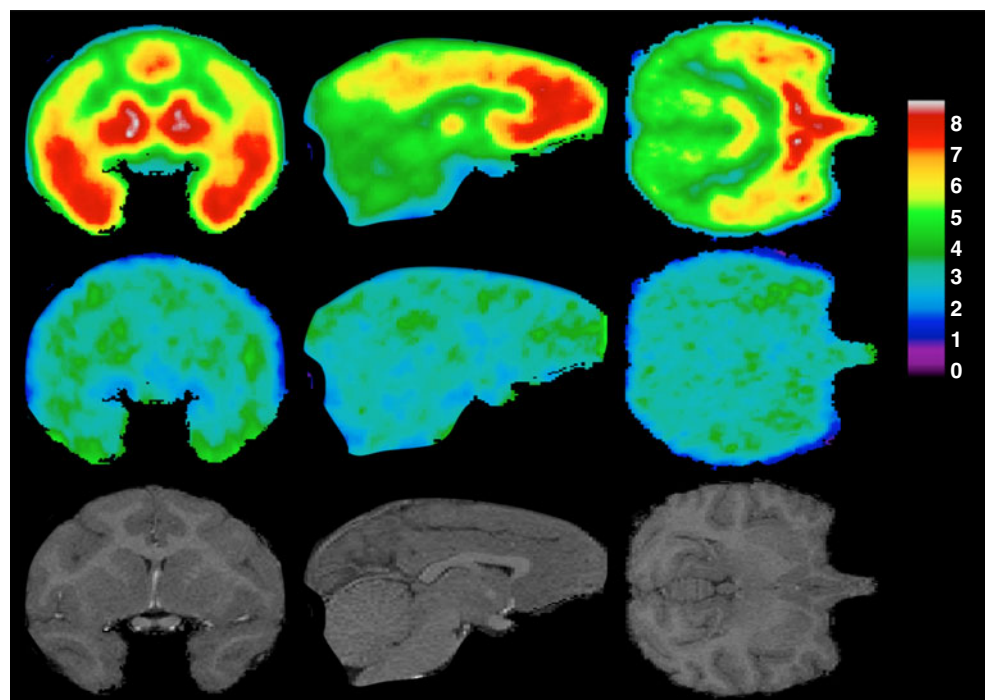
Table 1 Outcome metric values for the test–retest data (n=3) using V_T with 120 min scan duration. The mean and standard deviations across all subjects and all regions (listed in Fig. 3, with the exception of the cerebellum) are shown. The model that attained the best result in each category is shown in bold

	2TC models			Logan graphical approach	LEGA
	Unconstrained	Constrained	Noniterative		
Percent difference (%)	**5.92±4.13**	6.84±4.40	6.36±4.65	8.19±4.35	7.72±4.17
WSMSS (ml/cm³)²	**0.08±0.03**	0.10±0.03	0.09±0.05	0.14±0.06	0.13±0.06
ICC	**0.87±0.08**	0.84±0.09	0.83±0.11	0.77±0.15	0.79±0.13
Variance (ml/cm³)	0.55±0.18	**0.55±0.17**	0.55±0.19	0.58±0.18	0.61±0.20
Identifiability (ml/cm³)	1.11±0.46	1.18±0.45	1.09±0.39	1.17±0.38	**1.08±0.32**

2TC two-tissue compartment, *ICC* intraclass correlation coefficient, *LEGA* likelihood estimation in graphical analysis, *WSMSS* within-subject mean sum of squares

The black bars of Fig. 3 indicate average regional post-block V_T values. In general, these values are comparable across regions. However, the average post-block V_T values of the high-binding insula and temporal lobe are 15.9% and 16.8% higher, respectively, than the average CGM post-block V_T value. All other regions attained average post-block V_T values within 14% of the average CGM post-block V_T value.

The cerebellar white matter was also evaluated for its potential as a reference region. However, the cerebellar white matter had a greater average baseline V_T value (3.01±0.75), percent block (−8.99±26.31%), and post-block V_T value (2.61±0.24) than the cerebellar gray matter (data not shown). Therefore, it was excluded from subsequent analysis.

On average, CGM V_T values decreased by about 7% from baseline due to the MTEP block. The magnitude of this change indicates that there may be specific binding in

the CGM, and therefore no ideal reference region for [¹¹C] ABP688. Because of this, occupancy was also evaluated using the graphical approach described by Lassen et al. [56] and recently expanded by Cunningham et al. [37]. Lassen et al. [56] showed that a linear relationship exists between $V_T^{BASELINE}$ (independent variable) and $V_T^{BASELINE}$ - V_T^{BLOCK} (dependent variable). With minimal assumptions (namely that nonspecific binding and occupancy are the same in all regions), it can be shown that the x-intercept of the Lassen plot is equal to the nonspecific binding, V_{ND}, and the slope of the Lassen plot is drug occupancy [37, 56].

The Lassen plot of the three test–block experiments is shown in Fig. 4. Since two test–block experiments were performed on baboon 1 with the same dose of MTEP (1 mg/kg), the baseline and block V_T values were averaged across the two experiments for that subject. Based on the regression lines used to fit the transformed data, the V_{ND}

Fig. 2 TACs of five regions under baseline (*black*) and block (*gray*) conditions. The activities in the insula (*INS*), amygdala (*AMY*), medial prefrontal cortex (*MED*), dorsal and lateral prefrontal cortex (*DOR*), and cerebellar gray matter (*CGM*) in one test–block study are plotted over time. The raw data (*symbols*) were fitted with an unconstrained 2TC model (*solid lines*). The MTEP block lowered activity in high-binding regions. Some reduction in activity in the cerebellar gray matter is also apparent
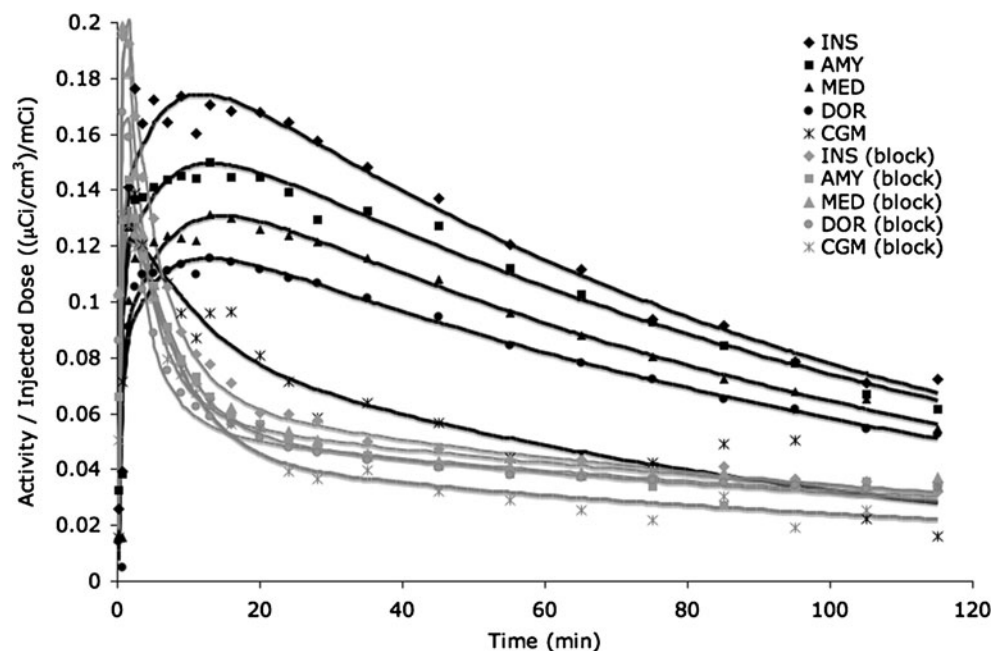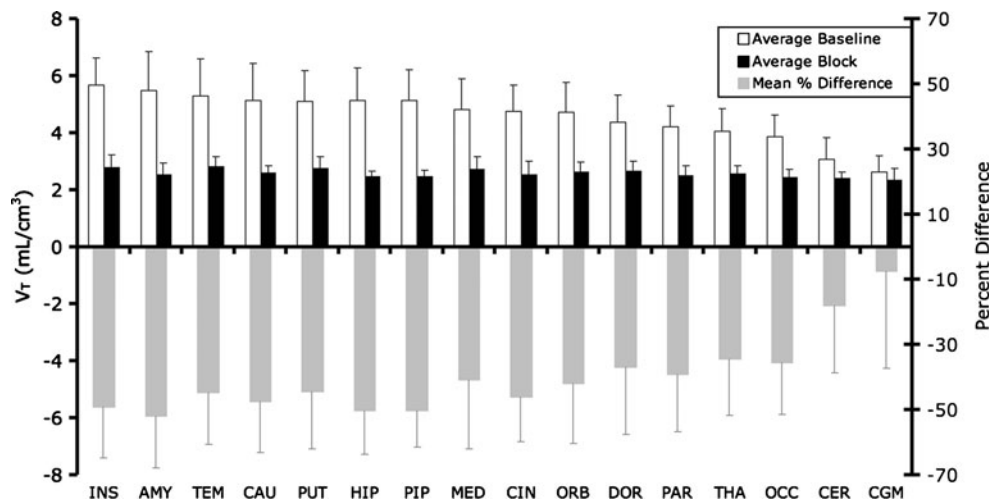
Fig. 3 Comparison of V_T in baseline ($n=3$) and block experiments ($n=3$). Baseline V_T values (*white bars*) are significantly higher than block V_T values (*black bars*). Regions are organized from left to right in order of highest to lowest mean baseline binding. The smallest difference between baseline and block conditions is seen in the cerebellar gray matter. Also shown is the percent difference in test– block pairs (*gray bars*). *INS* insula, *AMY* amygdala, *TEM* temporal lobe, *CAU* caudate, *PUT* putamen, *HIP* hippocampus, *PIP* para-hippocampal gyrus, *MED* medial prefrontal cortex, *CIN* cingulate, *ORB* orbital prefrontal cortex, *DOR* dorsal and lateral prefrontal cortex, *PAR* parietal lobe, *THA* thalamus, *OCC* occipital lobe, *CER* cerebellum, *CGM* cerebellar gray matter

values were estimated as 2.35 ml/cm^3 and 2.27 ml/cm^3, and the estimated percent occupancy was 88% and 91% for baboons 1 and 2, respectively.

Reference tissue approaches

Due to their expense and discomfort for the subject, it is sometimes preferable to perform a PET scan without an arterial line and plasma analysis. When plasma analysis is not available, reference region approaches must be used. These approaches require a reference region devoid of specific binding, which as mentioned above, does not exist for [^{11}C]ABP688. Therefore, it is important to evaluate the effects of a non-ideal reference region on the binding (and therefore occupancy) estimations of these modeling techniques.

To determine which reference region approach provides results most similar to those obtained when full compartment modeling is used, BP$_{ND}$ calculated using two reference tissue methods was plotted versus BP$_{ND}$ values calculated using the 2TC method (Fig. 5). When linear regression was performed on these two sets of data, the results were similar. However, due to the higher variance of the SRTM results, the bloodless version of the Logan graphical approach attained a higher R^2 value (0.98).

Test–retest and test–block results using multiple outcome measures

Figures 2–4 indicate that a significant block of [^{11}C] ABP688 binding was achieved with MTEP. Combined

with the low test–retest variability, these results indicate that [^{11}C]ABP688 is a promising tracer for in vivo imaging and occupancy studies. However, the lack of an ideal reference region may be problematic for studies in which arterial lines are not used. For these reasons, the use of [^{11}C]ABP688 in future studies will require decisions about appropriateness of the outcome measure. These choices may vary depending on each study's purpose and constraints, and it is therefore important to examine average values, test–retest reliability, and average percent block for multiple outcome measures. These values, presented in Table 2, were calculated using three possible outcome measures: V_T and BP$_P$ (using the 2TC modeling method), and BP$_{ND}$ (using the bloodless version of the Logan graphical approach).

Discussion

Modeling method comparison

It has been shown in humans that 2TC modeling methods fit [^{11}C]ABP688 data better than one-tissue compartment modeling methods, while the benefits of adding a constraint to the 2TC methods are less clear [34]. In addition, the Logan graphical approach has previously been shown to produce similar results to 2TC methods [34]. However, none of these approaches has been compared in a test–retest paradigm, which provides a standard for model comparisons and estimates of intraindividual binding needed to interpret occupancy results.
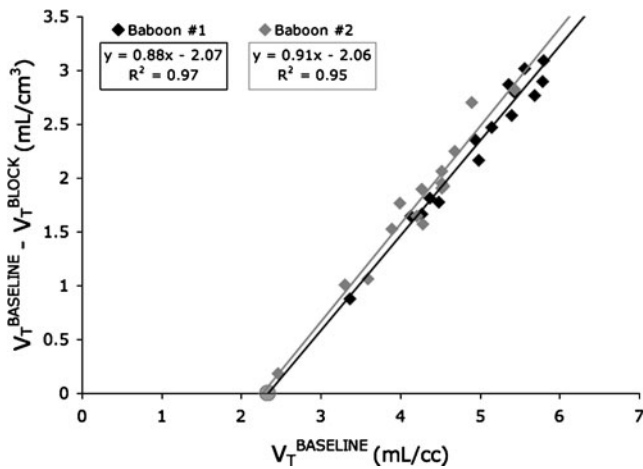
Fig. 4 Lassen plot. The data for baboon 1 (*black diamonds*) are the averages of two test–block studies, while the data for baboon 2 (*gray diamonds*) are from one study. The equations and goodness of fit of the regression lines (*gray* and *black lines*) are indicated in the boxes. Fitted slopes represent the estimated occupancy, which is assumed constant over all regions. The *x*-intercept of the regression lines, 2.35 and 2.27 ml/cm³ for baboons 1 and 2, respectively, is an estimate of nonspecific binding. The average post-block V_T value of the cerebellar gray matter is indicated by the *gray circle* (2.33 ml/cm³). This ROI was not included in the regression analysis

Based on the test–retest results (Table 1), the unconstrained 2TC modeling method was confirmed as optimal. This method produced good fits of the TAC data and stable outcome measures between test and retest, with the average V_T percent difference varying between 4.3 and 8.2% across all regions (Table 2). The unconstrained 2TC modeling method also produced outcome measures with low

WSMSS, variance, and identifiability, and high ICC (Table 1), indicating that outcome measures were highly reliable with low variability.

In vivo specificity for mGluR5

Prior studies have demonstrated that MPEP blocks [11C] ABP688 binding in rodents [29, 31, 32]. Although MPEP is a potent, noncompetitive mGluR5 antagonist, it has several drawbacks, including off-target affinity for other receptors such as mGluR4 [39, 57, 58]. Therefore, MTEP, with its high affinity for mGluR5 and superior selectivity relative to other receptors, was used in this study [39, 59]. The results of these test–block experiments suggest that [11C]ABP688 is sensitive to blockade of specific binding by MTEP and that this displacement is measurable by in vivo PET.

In this study, estimates of occupancy based on the Lassen plot appeared to be more reliable than those predicted using individual ROIs, for several reasons. First, the *x*-intercept of the Lassen plot provided validation of its estimates. The average of the Lassen plot *x*-intercept values (2.31 ml/cm³) is within 1% of the average post-block CGM V_T value (2.33 ml/cm³), though this region was not included in the Lassen plot regression analysis. The close agreement between these numbers provides confidence in the Lassen plot estimates, whereas the ROI-based estimates had no such validation. Second, occupancy estimates based on individual ROIs were significantly lower than the occupancy predicated by the Lassen plot (88–91%). However, individual ROI post-block V_T values were close
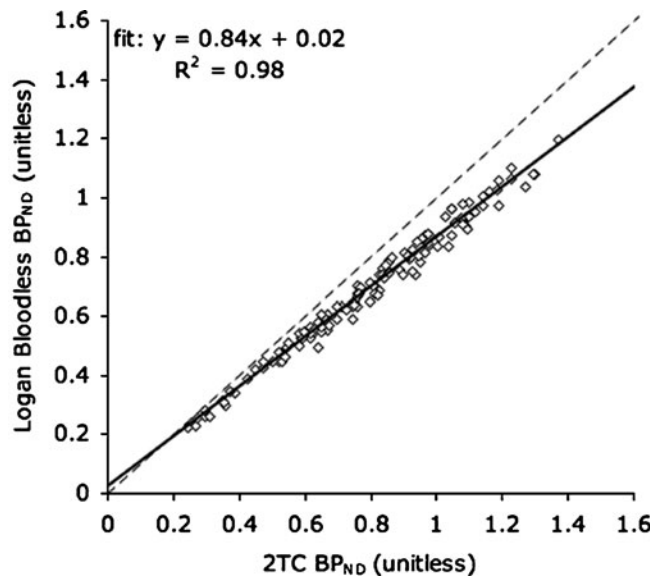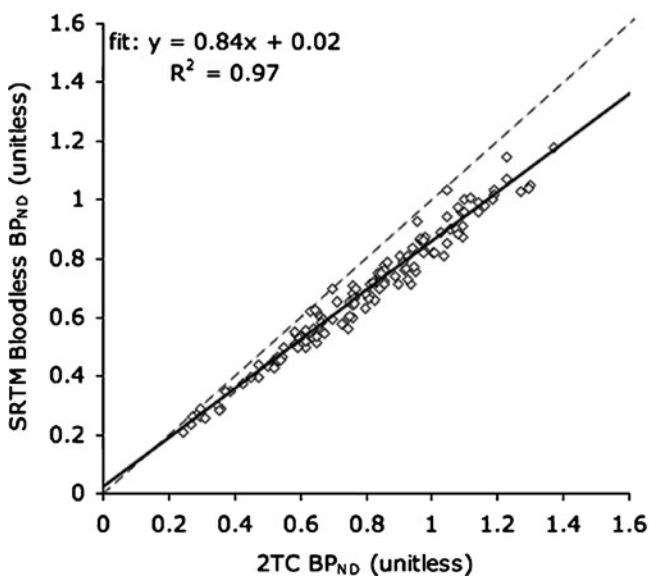

Fig. 5 BP_{ND} values calculated using the 2TC method with plasma input versus BP_{ND} values calculated by reference region approaches for baboon studies under normal conditions (*n*=9) using a scan duration of 120 min. Cerebellar gray matter was used as the reference

region. All high-binding ROIs listed in Fig. 3 are included. The slope, intercept and a measure of the goodness of fit (R^2) of the regression line are indicated. Identity lines are plotted (*dashed lines*) for reference

Table 2 Test–retest and test–block experiments using V_T, BP_P, and BP_{ND}. V_T averages and ranges were calculated over all regions, except for the reference region (cerebellar gray matter), which is listed separately. V_T and BP_P values were calculated over all high-binding regions using an arterial input function and an unconstrained 2TC modeling method. BP_{ND} values were calculated using the Logan graphical approach, without blood input information

Outcome measure	Region		Baseline scans (n=9)	Test–retest study, percent difference (n=6)	Test–block study, percent block (n=6)
V_T	All regions	Average±SD	5.14±0.99 ml/cm³	5.9±4.3%	−40.5±18.5%
		Range	4.01 : 6.06 ml/cm³	4.3 : 8.2%	−34.0 : −51.7%
	Cerebellar gray matter	Average±SD	2.90±0.62 ml/cm³	6.0±0.7%	−7.1±30.0%
BP_P	All regions	Average±SD	2.24±0.70 ml/cm³	11.7±6.1%	−83.5±15.0%
		Range	1.11 : 3.16 ml/cm³	4.4 : 17.7%	−76.3 : −90.8%
BP_{ND}	All regions	Average±SD	0.79±0.26	11.5±7.0%	−80.3±15.5%
		Range	0.39 : 1.12	6.3 : 15.8%	−72.4 : −88.2%

to the value of nonspecific binding (2.31 ml/cm³), indicating that an almost complete block was achieved in many regions. Therefore, higher occupancy estimates are more likely to be accurate. Lastly, and most importantly, an ideal reference region (i.e. a region completely devoid of specific binding) does not exist for [11C]ABP688. Because of this, reference region binding was affected by MTEP administration, leading to an underestimation of occupancy based on BP_P or BP_{ND}. However, since it was designed to provide accurate occupancy estimates even in the absence of an ideal reference region, occupancy underestimation is not an issue with the Lassen plot [37, 56].

Although estimates of occupancy based on V_T (Table 2) are not affected by the lack of an ideal reference region, these values were also lower than the occupancy values calculated using the Lassen plot (Fig. 4). This is mostly likely an artifact of the nonspecific binding. Since the average V_T value in the highest binding region, the insula, was only 6.1 ml/cm³, a good proportion (39–58%) of each ROI's V_T value was comprised of nonspecific binding. This nonspecific binding, which is not expected to change with administration of MTEP, can mask the effects of the specific binding changes, resulting in an underestimated occupancy.

Regardless of the method used to quantify it, however, the occupancy achieved by MTEP in these studies was significant. The significant blocking effect is particularly compelling in light of the low test–retest variance. This is an important finding because it establishes for the first time the sensitivity of [11C]ABP688 binding to MTEP administration. While sensitivity to MTEP administration does not exclude the possibility of [11C]ABP688 specifically binding to receptors other than mGluR5, the dramatic binding decrease between baseline and block scans, and the post-block volumes of distribution (which were similarly very low across all regions, consistent with the residual binding being nonspecific) indicate the in vivo selectivity of [11C]

ABP688 for mGluR5 in primates. This corroborates the findings of both in vitro human [26] and in vivo rodent studies [29, 31, 32]. Despite these initial in vitro and rodent studies, it was important to establish that in vivo PET can detect an MTEP blockade prior to performing similar studies in humans, due to the possible side effects of administering the mGluR5 antagonist needed for these studies.

Reference region determination

Of all the ROIs examined, the CGM had the lowest baseline V_T, the lowest post-block V_T, and the lowest average percent change in V_T between baseline and block experiments (Fig. 3). It is therefore a better candidate for reference region than the other regions tested, including both the full cerebellum and cerebellar white matter. The low estimates of binding in the CGM (and cerebellum) are in agreement with prior human [33, 34] and animal studies [26, 32, 60]. Consequently, the CGM appears to be the best possible choice for reference region. However, gray matter was stringently defined in this work, resulting in a small region of 103 mm³ on average (compared to the mean of 8420 mm³ full cerebellum). Because of this, CGM TACs were noisy, especially during the block, due to the lowered activity in that region. This led to a large standard deviation in the CGM V_T block estimate (large error bars for the percent difference in Fig. 3), and likely contributed to the large standard deviations in the block estimates using BP_P and BP_{ND} (Table 2). In addition, some of the calculated BP_P and BP_{ND} values were negative, most likely due to a slight overestimation CGM binding. (These values were set to zero for the test–block analysis.) In human studies, however, variance in CGM binding estimates is less likely to be a problem because the same stringent definition would result in a greater volume.

Although baboon CGM TACs are noisier than the full cerebellum TACs, the results of this study suggest that

CGM is still the appropriate reference region choice. The average V_T value of the full cerebellum was calculated as 3.27 ml/cm^3 (as opposed to the 2.90 ml/cm^3 of the CGM), with 2.31 ml/cm^3 (according to the Lassen plot) due to specific binding. This suggests that about 30% of the total binding in the full cerebellum is specific, confirming the existence of mGluR5 in mammalian cerebellum, as found by Patel et al. [61]. This specific binding can greatly compromise occupancy estimates, or group comparisons. In contrast, only about 20% of CGM binding is specific binding, based on the average CGM V_T value. However, the specific binding in the CGM (though much reduced compared to the full cerebellum) may still affect binding estimates using reference region approaches, as evidenced by the lower BP$_{ND}$ values in Fig. 5. Because of this, arterial lines and plasma analysis may be required for studies in which percent occupancy, or group differences, are expected to be minimal. If arterial lines are not used, it is possible that measured occupancy or group differences could be artifacts of the specific binding variation in the reference region.

Reference region approaches

Evaluation of reference region approaches revealed that BP$_{ND}$ values estimated using these models were lower, in general, than BP$_{ND}$ values estimated with the unconstrained 2TC method, leading to an underestimation of [^{11}C]ABP688 occupancy. This was mostly likely due to specific binding in the reference region (see above). Since the Logan reference tissue method produced data with a small spread about the regression line (high R^2), this modeling method appears to be a feasible reference tissue approach. This is in good agreement with previous work, in which results using the 2TC and Logan reference methods have been found to be similar [34]. However, the slopes and intercepts of the regression lines depicted in Fig. 5 were the same for BP$_{ND}$ values calculated using either the SRTM or the Logan bloodless approach. Therefore, SRTM also represents a reasonable reference tissue modeling alternative.

Conclusion

Performing both test–retest and test–block analyses allowed assessment of [^{11}C]ABP688 within-subject variability and the specificity of this ligand for mGluR5. The results of the test–retest study indicate that this ligand has low variability, and that the optimal modeling technique for [^{11}C]ABP688 with arterial input is the unconstrained 2TC modeling method. The results of the test–block study suggest that the specificity of [^{11}C]ABP688 is high, and that ligand binding can be effectively blocked by the

highly specific mGluR5 antagonist MTEP. Due to the lack of an ideal reference region, the graphical approach appears to be the optimal way to assess mGluR5 occupancy. Based on these results, occupancy studies of mGluR5 using [^{11}C]ABP688 appear to be feasible in baboon (and potentially human) studies. Since this receptor has been implicated in the pathophysiology of several neuropsychiatric disorders, [^{11}C]ABP688 may be of great value in the study of these disorders, as well as in the investigation of new therapeutic drugs.

References

1. Siegel GJ. Basic neurochemistry: molecular, cellular, and medical aspects. 7th ed. Amsterdam: Elsevier; 2006.
2. Palucha A, Pilc A. Metabotropic glutamate receptor ligands as possible anxiolytic and antidepressant drugs. Pharmacol Ther. 2007;115:116–47. doi:10.1016/j.pharmthera.2007.04.007.
3. Niswender CM, Conn PJ. Metabotropic glutamate receptors: physiology, pharmacology, and disease. Annu Rev Pharmacol Toxicol. 2010;50:295–322. doi:10.1146/annurev.pharmtox.011008.145533.
4. Spooren W, Ballard T, Gasparini F, Amalric M, Mutel V, Schreiber R. Insight into the function of group I and group II metabotropic glutamate (mGlu) receptors: behavioural characterization and implications for the treatment of CNS disorders. Behav Pharmacol. 2003;14:257–77. doi:10.1097/01.fbp.0000081783.35927.8f.
5. Lindsley CW, Shipe WD, Wolkenberg SE, Theberge CR, Williams Jr DL, Sur C, et al. Progress towards validating the NMDA receptor hypofunction hypothesis of schizophrenia. Curr Top Med Chem. 2006;6:771–85.
6. Liu F, Grauer S, Kelley C, Navarra R, Graf R, Zhang G, et al. ADX47273 [S-(4-fluoro-phenyl)-{3-[3-(4-fluoro-phenyl)-[1,2,4]-oxadiazol-5-yl]-piperidin-1-yl}-methanone]: a novel metabotropic glutamate receptor 5-selective positive allosteric modulator with preclinical antipsychotic-like and procognitive activities. J Pharmacol Exp Ther. 2008;327:827–39. doi:10.1124/jpet.108.136580.
7. Marino MJ, Conn PJ. Direct and indirect modulation of the N-methyl D-aspartate receptor. Curr Drug Targets CNS Neurol Disord. 2002;1:1–16.
8. Gass JT, Osborne MP, Watson NL, Brown JL, Olive MF. MGluR5 antagonism attenuates methamphetamine reinforcement and prevents reinstatement of methamphetamine-seeking behavior in rats. Neuropsychopharmacology. 2009;34:820–33. doi:10.1038/npp.2008.140.
9. Markou A. Accruing preclinical evidence about metabotropic glutamate 5 receptor antagonists as treatments for drug dependence highlights the irreplaceable contributions of animal studies to the discovery of new medications for human disorders. Neuropsychopharmacology. 2009;34:817–9. doi:10.1038/Npp.2008.218.
10. Aguirre JA, Kehr J, Yoshitake T, Liu FL, Rivera A, Fernandez-Espinola S, et al. Protection but maintained dysfunction of nigral dopaminergic nerve cell bodies and striatal dopaminergic terminals in MPTP-lesioned mice after acute treatment with the

mGluR5 antagonist MPEP. Brain Res. 2005;1033:216–20. doi:10.1016/j.brainres.2004.11.040.

11. Domenici MR, Potenza RL, Martire A, Coccurello R, Pezzola A, Reggio R, et al. Chronic treatment with the mGlu5R antagonist MPEP reduces the functional effects of the mGlu5R agonist CHPG in the striatum of 6-hydroxydopamine-lesioned rats: possible relevance to the effects of mGlu5R blockade in Parkinson's disease. J Neurosci Res. 2005;80:646–54. doi:10.1002/jnr.20489.

12. Turle-Lorenzo N, Breysse N, Baunez C, Amalric M. Functional interaction between mGlu 5 and NMDA receptors in a rat model of Parkinson's disease. Psychopharmacology (Berl). 2005;179:117–27. doi:10.1007/s00213-005-2202-x.

13. Elia J, Gai X, Xie HM, Perin JC, Geiger E, Glessner JT, et al. Rare structural variants found in attention-deficit hyperactivity disorder are preferentially associated with neurodevelopmental genes. Mol Psychiatry. 2010;15:637–46. doi:10.1038/mp.2009.57.

14. Aronica E, Gorter JA, Jansen GH, van Veelen CW, van Rijen PC, Ramkema M, et al. Expression and cell distribution of group I and group II metabotropic glutamate receptor subtypes in taylor-type focal cortical dysplasia. Epilepsia. 2003;44:785–95.

15. Dolen G, Bear MF. Role for metabotropic glutamate receptor 5 (mGluR5) in the pathogenesis of fragile X syndrome. J Physiol. 2008;586:1503–8. doi:10.1113/jphysiol.2008.150722.

16. Kanuma K, Aoki T, Shimazaki Y. Recent patents on positive allosteric modulators of the metabotropic glutamate 5 receptor as a potential treatment for schizophrenia. Recent Pat CNS Drug Discov. 2010;5:23–34.

17. Stefani MR, Moghaddam B. Activation of type 5 metabotropic glutamate receptors attenuates deficits in cognitive flexibility induced by NMDA receptor blockade. Eur J Pharmacol. 2010;639:26–32. doi:10.1016/j.ejphar.2010.01.028.

18. Dolen G, Carpenter RL, Ocain TD, Bear MF. Mechanism-based approaches to treating fragile X. Pharmacol Ther. 2010;127:78–93. doi:10.1016/j.pharmthera.2010.02.008.

19. Steru L, Chermat R, Thierry B, Simon P. The tail suspension test: a new method for screening antidepressants in mice. Psychopharmacology (Berl). 1985;85:367–70.

20. Porsolt RD, Anton G, Blavet N, Jalfre M. Behavioural despair in rats: a new model sensitive to antidepressant treatments. Eur J Pharmacol. 1978;47:379–91.

21. Belozertseva IV, Kos T, Popik P, Danysz W, Bespalov AY. Antidepressant-like effects of mGluR1 and mGluR5 antagonists in the rat forced swim and the mouse tail suspension tests. Eur Neuropsychopharmacol. 2007;17:172–9.

22. Palucha A, Branski P, Szewczyk B, Wieronska JM, Klak K, Pilc A. Potential antidepressant-like effect of MTEP, a potent and highly selective mGluR5 antagonist. Pharmacol Biochem Behav. 2005;81:901–6.

23. Li X, Need AB, Baez M, Witkin JM. Metabotropic glutamate 5 receptor antagonism is associated with antidepressant-like effects in mice. J Pharmacol Exp Ther. 2006;319:254–9. doi:10.1124/jpet.106.103143.

24. Pilc A, Klodzinska A, Branski P, Nowak G, Palucha A, Szewczyk B, et al. Multiple MPEP administrations evoke anxiolytic- and antidepressant-like effects in rats. Neuropharmacology. 2002;43:181–7.

25. Wieronska JM, Szewczyk B, Branski P, Palucha A, Pilc A. Antidepressant-like effect of MPEP, a potent, selective and systemically active mGlu5 receptor antagonist in the olfactory bulbectomized rats. Amino Acids. 2002;23:213–6. doi:10.1007/s00726-001-0131-5.

26. Hintermann S, Vranesic I, Allgeier H, Brulisauer A, Hoyer D, Lemaire M, et al. ABP688, a novel selective and high affinity ligand for the labeling of mGlu5 receptors: identification, in vitro pharmacology, pharmacokinetic and biodistribution studies. Bioorg Med Chem. 2007;15:903–14.

27. Porter RH, Jaeschke G, Spooren W, Ballard TM, Buttelmann B, Kolczewski S, et al. Fenobam: a clinically validated nonbenzodiazepine anxiolytic is a potent, selective, and noncompetitive mGlu5 receptor antagonist with inverse agonist activity. J Pharmacol Exp Ther. 2005;315:711–21.

28. Pecknold JC, McClure DJ, Appeltauer L, Wrzesinski L, Allan T. Treatment of anxiety using fenobam (a nonbenzodiazepine) in a double-blind standard (diazepam) placebo-controlled study. J Clin Psychopharmacol. 1982;2:129–33.

29. Ametamey SM, Kessler LJ, Honer M, Wyss MT, Buck A, Hintermann S, et al. Radiosynthesis and preclinical evaluation of 11C-ABP688 as a probe for imaging the metabotropic glutamate receptor subtype 5. J Nucl Med. 2006;47:698–705.

30. Gasparini F, Andres H, Flor PJ, Heinrich M, Inderbitzin W, Lingenhohl K, et al. [(3)H]-M-MPEP, a potent, subtype-selective radioligand for the metabotropic glutamate receptor subtype 5. Bioorg Med Chem Lett. 2002;12:407–9.

31. Elmenhorst D, Minuzzi L, Aliaga A, Rowley J, Massarweh G, Diksic M, et al. In vivo and in vitro validation of reference tissue models for the mGluR(5) ligand [(11)C]ABP688. J Cereb Blood Flow Metab. 2010;30:1538–49. doi:10.1038/jcbfm.2010.65.

32. Wyss MT, Ametamey SM, Treyer V, Bettio A, Blagoev M, Kessler LJ, et al. Quantitative evaluation of 11C-ABP688 as PET ligand for the measurement of the metabotropic glutamate receptor subtype 5 using autoradiographic studies and a beta-scintillator. Neuroimage. 2007;35:1086–92. doi:10.1016/j.neuroimage.2007.01.005.

33. Ametamey SM, Treyer V, Streffer J, Wyss MT, Schmidt M, Blagoev M, et al. Human PET studies of metabotropic glutamate receptor subtype 5 with 11C-ABP688. J Nucl Med. 2007;48:247–52.

34. Treyer V, Streffer J, Wyss MT, Bettio A, Ametamey SM, Fischer U, et al. Evaluation of the metabotropic glutamate receptor subtype 5 using PET and 11C-ABP688: assessment of methods. J Nucl Med. 2007;48:1207–15. doi:10.2967/jnumed.107.039578.

35. Johnson MP, Nisenbaum ES, Large TH, Emkey R, Baez M, Kingston AE. Allosteric modulators of metabotropic glutamate receptors: lessons learnt from mGlu1, mGlu2 and mGlu5 potentiators and antagonists. Biochem Soc Trans. 2004;32:881–7. doi:10.1042/BST0320881.

36. Ritzen A, Mathiesen JM, Thomsen C. Molecular pharmacology and therapeutic prospects of metabotropic glutamate receptor allosteric modulators. Basic Clin Pharmacol Toxicol. 2005;97:202–13. doi:10.1111/j.1742-7843.2005.pto_156.x.

37. Cunningham VJ, Rabiner EA, Slifstein M, Laruelle M, Gunn RN. Measuring drug occupancy in the absence of a reference region: the Lassen plot re-visited. J Cereb Blood Flow Metab. 2010;30:46–50. doi:10.1038/jcbfm.2009.190.

38. Milak MS, Ogden RT, Vinocur DN, Van Heertum RL, Cooper TB, Mann JJ, et al. Effects of tryptophan depletion on the binding of [11C]-DASB to the serotonin transporter in baboons: response to acute serotonin deficiency. Biol Psychiatry. 2005;57:102–6. doi:10.1016/j.biopsych.2004.09.026.

39. Busse CS, Brodkin J, Tattersall D, Anderson JJ, Warren N, Tehrani L, et al. The behavioral profile of the potent and selective mGlu5 receptor antagonist 3-[(2-methyl-1, 3-thiazol-4-yl)ethynyl] pyridine (MTEP) in rodent models of anxiety. Neuropsychopharmacology. 2004;29:1971–9.

40. Anderson JJ, Bradbury MJ, Giracello DR, Chapman DF, Holtz G, Roppe J, et al. In vivo receptor occupancy of mGlu5 receptor antagonists using the novel radioligand [3H]3-methoxy-5-(pyridin-2-ylethynyl)pyridine). Eur J Pharmacol. 2003;473:35–40.

41. Stachowicz K, Golembiowska K, Sowa M, Nowak G, Chojnacka-Wojcik E, Pilc A. Anxiolytic-like action of MTEP expressed in the conflict drinking Vogel test in rats is serotonin dependent. Neuropharmacology. 2007;53:741–8. doi:10.1016/j.neuropharm.2007.08.002.

42. DeLorenzo C, Kumar JSD, Zanderigo F, Mann JJ, Parsey RV. Modeling considerations for in vivo quantification of the dopamine transporter using [C-11]PE2I and positron emission tomography. J Cereb Blood Flow Metab. 2009;29:1332–45. doi:10.1038/Jcbfm.2009.49.

43. Ogden RT, Ojha A, Erlandsson K, Oquendo MA, Mann JJ, Parsey RV. In vivo quantification of serotonin transporters using [(11)C] DASB and positron emission tomography in humans: modeling considerations. J Cereb Blood Flow Metab. 2007;27:205–17. doi:10.1038/sj.jcbfm.9600329.

44. Kwon Y. Handbook of essential pharmacokinetics, pharmacodynamics, and drug metabolism for industrial scientists. New York: Kluwer Academic/Plenum Publishers; 2001.

45. Lohman JJHM. Plasma-protein binding of drugs – implications for therapeutic drug-monitoring. Pharm Weekbl Sci Ed. 1986;8:302–4.

46. Gunn RN, Sargent PA, Bench CJ, Rabiner EA, Osman S, Pike VW, et al. Tracer kinetic modeling of the 5-HT1A receptor ligand [carbonyl-11C]WAY-100635 for PET. Neuroimage. 1998;8:426–40. doi:10.1006/nimg.1998.0379.

47. Innis RB, Cunningham VJ, Delforge J, Fujita M, Gjedde A, Gunn RN, et al. Consensus nomenclature for in vivo imaging of reversibly binding radioligands. J Cereb Blood Flow Metab. 2007;27:1533–9. doi:10.1038/sj.jcbfm.9600493.

48. Parsey RV, Slifstein M, Hwang DR, Abi-Dargham A, Simpson N, Mawlawi O, et al. Validation and reproducibility of measurement of 5-HT1A receptor parameters with [carbonyl-11C]WAY-100635 in humans: comparison of arterial and reference tissue input functions. J Cereb Blood Flow Metab. 2000;20:1111–33. doi:10.1097/00004647-200007000-00011.

49. Logan J, Fowler JS, Volkow ND, Wolf AP, Dewey SL, Schlyer DJ, et al. Graphical analysis of reversible radioligand binding from time-activity measurements applied to [N-11C-methyl]-(-)-cocaine PET studies in human subjects. J Cereb Blood Flow Metab. 1990;10:740–7.

50. Slifstein M, Laruelle M. Effects of statistical noise on graphic analysis of PET neuroreceptor studies. J Nucl Med. 2000;41:2083–8.

51. Ogden RT. Estimation of kinetic parameters in graphical analysis of PET imaging data. Stat Med. 2003;22:3557–68. doi:10.1002/sim.1562.

52. Lammertsma AA, Hume SP. Simplified reference tissue model for PET receptor studies. Neuroimage. 1996;4:153–8.

53. Logan J, Fowler JS, Volkow ND, Wang GJ, Ding YS, Alexoff DL. Distribution volume ratios without blood sampling from graphical analysis of PET data. J Cereb Blood Flow Metab. 1996;16:834–40.

54. Ogden RT, Tarpey T. Estimation in regression models with externally estimated parameters. Biostatistics. 2006;7:115–29. doi:10.1093/biostatistics/kxi044.

55. Ardekani BA, Guckemus S, Bachman A, Hoptman MJ, Wojtaszek M, Nierenberg J. Quantitative comparison of algorithms for inter-subject registration of 3D volumetric brain MRI scans. J Neurosci Methods. 2005;142:67–76. doi:10.1016/j.jneumeth.2004.07.014.

56. Lassen NA, Bartenstein PA, Lammertsma AA, Prevett MC, Turton DR, Luthra SK, et al. Benzodiazepine receptor quantification in-vivo in humans using [C-11] flumazenil and PET – application of the steady-state principle. J Cereb Blood Flow Metab. 1995;15:152–65.

57. Cosford ND, Tehrani L, Roppe J, Schweiger E, Smith ND, Anderson J, et al. 3-[(2-Methyl-1,3-thiazol-4-yl)ethynyl]-pyridine: a potent and highly selective metabotropic glutamate subtype 5 receptor antagonist with anxiolytic activity. J Med Chem. 2003;46:204–6. doi:10.1021/jm025570j.

58. Mathiesen JM, Svendsen N, Brauner-Osborne H, Thomsen C, Ramirez MT. Positive allosteric modulation of the human metabotropic glutamate receptor 4 (hmGluR4) by SIB-1893 and MPEP. Br J Pharmacol. 2003;138:1026–30. doi:10.1038/sj.bjp. 0705159.

59. Cosford ND, Roppe J, Tehrani L, Schweiger EJ, Seiders TJ, Chaudary A, et al. [3H]-methoxymethyl-MTEP and [3H]-methoxy-PEPy: potent and selective radioligands for the metabotropic glutamate subtype 5 (mGlu5) receptor. Bioorg Med Chem Lett. 2003;13:351–4.

60. Honer M, Stoffel A, Kessler LJ, Schubiger PA, Ametamey SM. Radiolabeling and in vitro and in vivo evaluation of [(18)F]-FE-DABP688 as a PET radioligand for the metabotropic glutamate receptor subtype 5. Nucl Med Biol. 2007;34:973–80.

61. Patel S, Hamill TG, Connolly B, Jagoda E, Li W, Gibson RE. Species differences in mGluR5 binding sites in mammalian central nervous system determined using in vitro binding with [18 F]F-PEB. Nucl Med Biol. 2007;34:1009–17. doi:10.1016/j. nucmedbio.2007.07.009.